The Modeling of the Absorbance of Sub-THz Radiation by Human Skin

Noa Betzalel, Yuri Feldman, and Paul Ben Ishai

***Abstract*—In the near future, applications will come online that require data transmission in ultrahigh rates of 100 Gbit per second and beyond. In fact, the planning for new industry regulations for the exploitation of the sub-THz band are well advanced under the auspices of IEEE 802.15 Terahertz Interest Group. One aspect of this endeavor is to gauge the possible impact on human health by the expected explosion in commercial use of this band. It is, therefore, imperative to estimate the respective specific absorption rates of human tissues. In the interaction of microwave radiation and human beings, the skin is traditionally considered as just an absorbing sponge stratum filled with water. This approach is justified when the impinging wavelength is greater than the dimensions of the skin layer. However, in the sub-THz band this condition is violated. In 2008, we demonstrated that the coiled portion of the sweat duct in upper skin layer could be regarded as a helical antenna in the sub-THz band. The full ramifications of what these findings represent in the human condition are still very unclear, but it is obvious that the absorption of electromagnetic energy is governed by the topology for the skin and its organelles, especially the sweat duct.**

***Index Terms*—5G, helical antenna, human skin, specific absorption rate (SAR), sub-terahertz (sub-THz), sweat duct.**

I. Introduction

IN THE near future, applications will come online which require data transmission in ultrahigh rates of 100 Gbit per second and beyond (see Fig. 1). In fact, the planning for new industry regulations for the exploitation of the sub-terahertz (sub-THz) band are well advanced under the auspices of IEEE 802.15 Terahertz Interest Group [1]. One aspect of this endeavor is to gauge the possible impact on human health by the expected explosion in commercial use of this band. It is, therefore, imperative to estimate the respective specific absorption rates (SARs) of human tissues. The industry accepted method to assess SARs is by the use of phantoms [2]–[4]. This can be justified when the wavelength of the impinging signal is greater than the dimensions of biological tissue involved or when the tissue can be considered as an infinite layer, compared to the wavelength. Under such conditions, one can consider the tissue as homogeneous and work with an artificial substitute having the same general dielectric properties. However, these conditions cannot be accepted as valid for sub-mm wavelengths, where the dimensions of tissues like skin are on a par with those same wavelengths [5], [6].

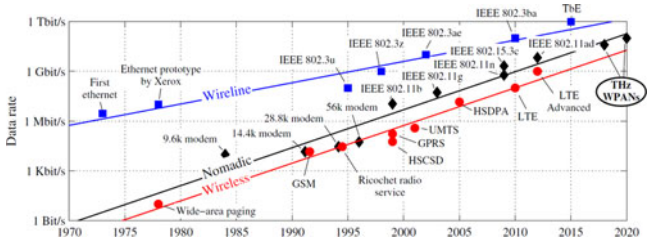

Fig. 1. Data-rates evolution in the wireless communication field (reproduced from [1], copyright (2013) Springer Publishing Company).

As an alternative to the use of phantoms, electromagnetic (EM) simulations software packages can be used. The more sophisticated of these are voxel-based models for the human anatomy [7]. They began to appear for EM studies in 2004 [8] and followed a similar development in MIR models [9]. The most sophisticated models today can achieve tissue resolutions of 1–2 mm and accurately describe the internal organs [10], [11]. While these techniques allow the calculation of SARs in body areas where it is impractical to measure, these models are still plagued by a lack of standardization [12], making comparative studies difficult. Although simulation is a far more flexible approach to the SARs problem, the voxel man approach can still mislead once the wavelength of interest approaches the minimum physical dimensions of the model elements. For instance, skin is a striated organ with layer dimensions one tenth of the smallest element in the Austin Man voxel model [10]. Phenomena such as standing wave absorption would consequently be overlooked and the effect of skin organelles having the same physical dimensions as the wavelength would be simply invisible.

We present a simulation model of the human skin, taking into account its multiple layers and the helical segment of the sweat duct. It was previously shown that the helically shaped structure of human sweat ducts, together with the dielectric properties of human skin, could be considered as an array of helical antennas, with a working bandwidth of a few hundreds of gigahertz and centered around 380 GHz [5], [13]. These findings have been confirmed by the existence of circular dichroism in the reflection coefficient of the human palm, measured at 380 GHz [13], [14] Furthermore, both simulation and experimental results show that

Manuscript received March 26, 2017; revised May 25, 2017 and July 8, 2017; accepted July 25, 2017. Date of publication August 25, 2017; date of current version September 13, 2017. *(Corresponding author: Paul Ben Ishai.)*

N. Betzalel and Y. Feldman are with the Department of Applied Physics, The Hebrew University of Jerusalem, Jerusalem 91904, Israel (e-mail: noa.betzalel@mail.huji.ac.il; yurif@mail.huji.ac.il).

P. Ben Ishai was with The Hebrew University of Jerusalem, Jerusalem 91904, Israel. He is now with the Department of Physics, Ariel University, Ariel 40700, Israel (e-mail: paulbi@ariel.ac.il).

Color versions of one or more of the figures in this paper are available online at http://ieeexplore.ieee.org.

Digital Object Identifier 10.1109/TTHZ.2017.2736345

2156-342X © 2017 IEEE. Personal use is permitted, but republication/redistribution requires IEEE permission.
See http://www.ieee.org/publications_standards/publications/rights/index.html for more information.

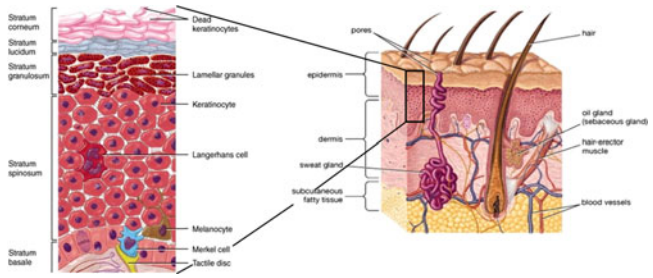

Fig. 2. Cross section of human skin. The three main layers, subcutaneous fatty tissue (hypodermis), dermis, and epidermis are shown, as well as the eccrine sweat gland (on the right). Epidermis' five substratum-layers: basale, spinosum, granulosum, lucidum, and corneum. (Reproduced from Pinterest and Encyclopedia Britanica, Inc.)

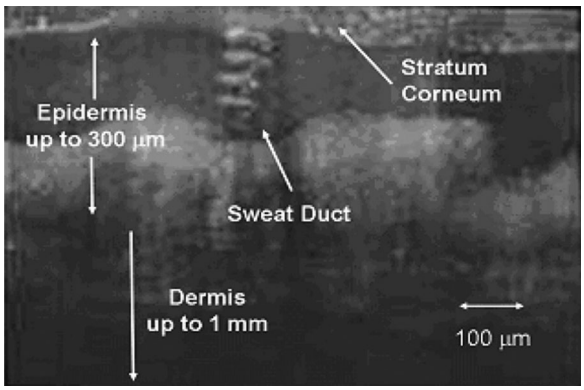

Fig. 3. Optical coherence tomography image of a human sweat duct *in vivo*. The coiled portion of the duct is clearly visible. (Reproduced with permission of Feldman *et al.* (2008); copyright 2008, American Physical Society).

the human skin absorbs radiation in the sub-THz frequencies region as a function of sweat duct activity [5], [6], [15], [16]. These results are extremely important if the explosion in sub-THz communications will occur in the next few years.

In the following sections, we will describe the structure of human skin as a multilayered construct, punctuated by coiled sweat ducts, and examine the water content of each element as the primary cause of sub-THz absorption. We will then describe a simulation model based on realistic parameters of the skin. Finally, the SARs' profile for human skin in the sub-THz regime presented and the implications are discussed.

II. Structure of Skin

Skin is not only the largest, but also, functionally, the most versatile organ of the human body. It consists of three main layers: epidermis, dermis, and subcutaneous fatty layer (hypodermis), illustrated in Fig. 2. As a platform for the perspiration system, the skin contains 2–5 million sweat glands [16]. They are located at the bottom of the dermis, and are deployed throughout the skin. OCT imaging of the human palm has revealed that the sweat duct in the upper epidermis is in fact coiled (see Fig. 3) with a mean diameter of about 90 μm [18]. The epidermis itself consists of five sublayers referred to as stratum layers [19], as shown in Fig. 2 on the left.

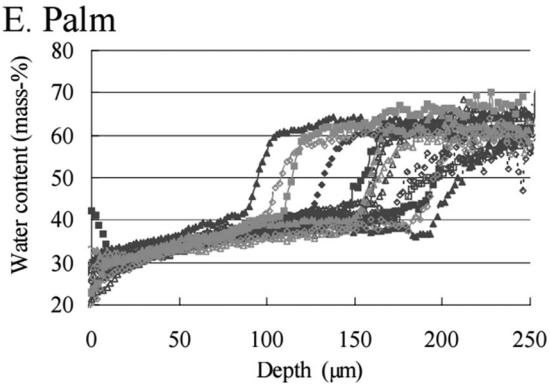

Fig. 4. Epidermis water concentration profile as a function of the palm skin's depth. Those measurements were made *in vivo*, where Raman spectra were obtained at different depths below the skin surface using a confocal Raman spectrometer. (Reproduced from [21]; copyright 2007, Advanced in Dermatology and Venereology).

The sublayers differ one from another in its keratinocyte cell concentration. The keratinocytes constitute 90% of the cells found in the epidermis. They are produced by cell division in the deepest layer of the epidermis – the basale layer and move progressively toward the skin surface. As they ascend, they undergo a process known as "terminal differentiation," in order to generate the surface layer of cells—the stratum cornea (SC), which is constituted of dead cells that are gradually abraded by daily wear and tear [20]. Thus, the live keratinocytes cells' concentration decreases as we move progressively toward the skin surface, leading to a water gradient throughout the epidermis layer. The water gradient has been measured [21] in the skin layer and it shows a distinct step, coinciding with the boundary between the epidermal layer and the dermis (see Fig. 4).

Recent studies reported that, together with the dielectric properties of the human skin, the helical structure of human eccrine sweat ducts has EM-properties that resemble to those of low Q-factor helical antennas. This is facilitated by the relatively high value of ac conductivity, σ ac of water above 100 GHz. In pure water, it has been measured at 100 S/m [22]. However, along the highly structured H-bond network commonly found at a lipid water interface [23], it can be far higher. In [13], it was shown that ac conductivity levels of 5000 S/m are not unreasonable due to this effect. The characteristic frequencies of such helical structures in the sub-THz frequency range are due to their helix diameter and helix length [5], [6], [14], [18], [24]. However, due to the water gradient of the surrounding tissue they are embedded in a nonuniform medium, i.e., nonuniform conductivity and permittivity. The influence of those water gradients on the axial mode frequency of the duct can be approximated by using an effective permittivity for the medium, according to the formula

$$f = \frac{c_0}{2\pi R\sqrt{\varepsilon_{\text{eff}}}}. \tag{1}$$

c_0 is the velocity of light in vacuum, R is the radius of the helical duct, and ε_{eff} is an effective dielectric permittivity, derived by a weighted average of all sublayer permittivity's, the mechanism of which is described below.

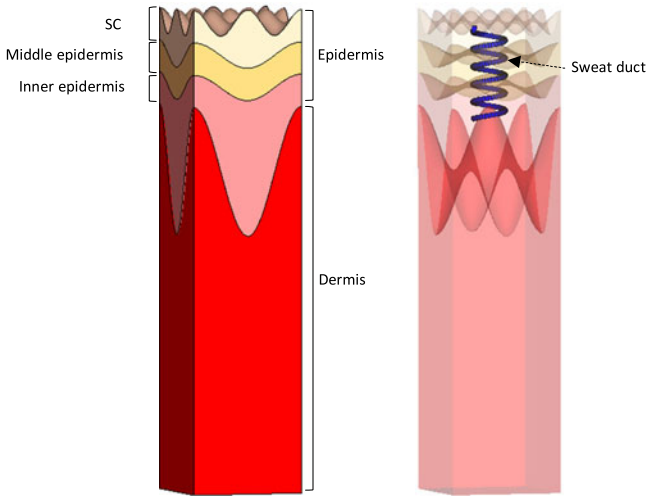

Fig. 5. Skin model. On the left: unit cell, consist of two main layers; dermis and epidermis. The epidermis consists of three sublayers; inner epidermis (IE), middle epidermis (ME), and SC. On the right: A transparent view of the unit cell form the left, to reveal its interiors, i.e., helical section of sweat duct.

II. Methods

A. Model

While the skin is a platform for a plethora of functional structures, such hair follicles and nociceptors, their physical dimensions and geometries do not render them sensitive to sub-THz radiation. Consequently, the model focuses on the sweat duct and treats the skin as a series of homogenous layers.

The model is a unit cell, which consist of two main layers; dermis and epidermis. We do not include the third main layer, hypodermis, because initial studies [13] demonstrate that THz radiation does not penetrate beyond the typical depth of the epidermis layer and consequently the hypodermis does not play an important role in shaping the EM spectral response. The boundary between the epidermis and the dermis acts as a reflection plane of the helical antenna, due to the disparity of the dielectric properties of the respective layers. The epidermis layer is further divided into three main layers, referred to as the inner epidermis, the middle epidermis, and the SC. The helical section of the sweat duct was embedded in the epidermis layer, as shown in the right-hand side of Fig. 5, to correspond with the position of the duct noted by OCT (see Fig. 3).

The boundary between the dermis and the epidermis was modeled as a two-dimensional (2-D) sinusoidal surface with an amplitude of 200 μm, which corresponds to the papillary dermis in human skin [14], [18], see Fig. 6 below. Although the moisture profile of skin as boundaries between the sublayers of the epidermis (middle and inner epidermis) were also modeled sinusoidally with amplitudes of 40 μm.

The dielectric permittivity of each layer was extracted from the data in Fig. 4, as can be seen in Fig. 7 below. It was calculated using the mixture formula presented in (4) of [6]

$$\varepsilon_{\text{layer}} = \varepsilon^{bm} \frac{\left(2\varepsilon^{bm} + \varepsilon^{w}\right) + 2\phi\left(\varepsilon^{bm} - \varepsilon^{w}\right)}{\left(2\varepsilon^{bm} + \varepsilon^{w}\right) + \phi\left(\varepsilon^{bm} - \varepsilon^{w}\right)} \qquad (2)$$

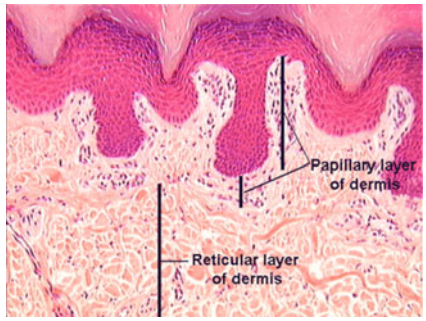

Fig. 6. Cross section of human skin. The papillary layer is clearly seen. Reproduced from cyhsanatomy1; copyright 2017, Tangient LLC.

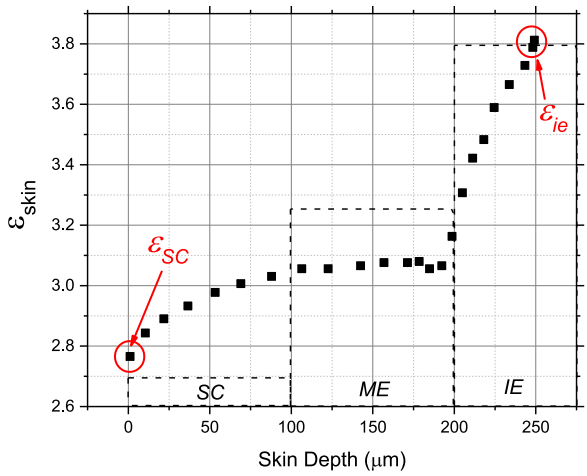

Fig. 7. Skin permittivity as a function of skin depth, calculated by (2), using the measured water content presented in Fig. 4. As the dielectric losses for water are small and for lipid almost flat in the frequency range, their values in (2) are taken as constant. $\varepsilon_{\text{SC}} \approx 2.7$ is the dielectric permittivity of the SC and $\varepsilon_{\text{ie}} \approx 3.8$ is the dielectric permittivity of the IE. The dashed lines represent the averaged values used in the layers constructed in the skin simulation model and described in Table I.

TABLE I
Estimated Skin Dielectric Permittivity and AC Conductivity

Component	Relative Permittivity	AC Conductivity (S/m)
Stratum Coenea (SC)	2.7	1
Middle Epidermis (ME)	3.25	0.5
Inner Epidermis (IE)	3.8	1
Dermis	3.9	30
Sweat duct wall	4	0.01

Estimated skin dielectric permittivity and ac conductivity, which were used in the simulations model. The ac conductivity of the sweat ducts is considered to be much higher than that of its surrounding epidermis.

where ε^{bm} is the permittivity of the dry biological structural components, approximately 2.2 [25], ε^{w} is a permittivity of water, and ϕ is the volume fraction of the water component [6], [25]. In the considered frequency range, dielectric losses for water are low and for the dry biological components are negligible. Consequently, the permittivity can be represented by a single, frequency independent value.

The model parameters are summarized in Table I and Fig. 8. The conductivity of the sweat ducts was considered to be much

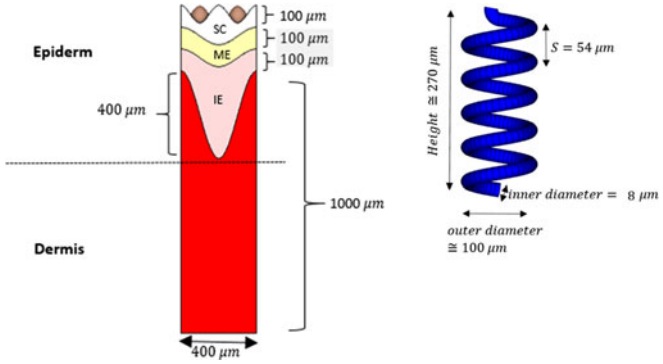

Fig. 8. On the left—the model side cross section. The skin is divided into four layers: SC, middle epidermis (ME), Inner epidermis (IE), and dermis. The helical sweat ducts are located in the epidermis. Sinusoidal functions with different spatial frequencies and amplitudes are used in order to model the nonflat boundaries between the dermis, IE, ME, and SC. On the right—the sweat duct dimensions.

higher than that of the skin layers, varying between zero in the absence of sweat duct activity to 100–11 000 S/m [5], [13].

Based on Fig. 7, the dielectric permittivity of the ME layer was considered to be the average of the dielectric permittivity of the layer above (i.e., SC) and the layer below [i.e., inner epidermis (IE)]

$$\varepsilon_{\mathrm{ME}} = \frac{1}{2}\varepsilon_{\mathrm{IE}} + \frac{1}{2}\varepsilon_{\mathrm{SC}} \approx 3.25. \tag{3}$$

In order to calculate the axial frequency of the duct, we constructed an effective dielectric permittivity from the weighted average of dielectric coefficients of all the layers in the epidermal region considered as series capacitances

$$\frac{1}{\varepsilon_{\mathrm{effective}}} = \phi_{\mathrm{IE}} \cdot \frac{1}{\varepsilon_{\mathrm{IE}}} + \phi_{\mathrm{ME}} \cdot \frac{1}{\varepsilon_{\mathrm{ME}}} + \phi_{\mathrm{SC}} \cdot \frac{1}{\varepsilon_{\mathrm{SC}}} \tag{4}$$

where ϕ_i is the relative volume of each layer, and is defined as follows:

$$\phi_i = \frac{H_i}{H_{\mathrm{IE}} + H_{\mathrm{ME}} + H_{\mathrm{SC}}}, \quad i = \mathrm{IE}, \mathrm{ME}, \mathrm{SC}. \tag{5}$$

Where H_i is the effective height of the layer. Replacing the vacuum dielectric permittivity ε_0 in (1) by $\varepsilon_{\mathrm{effective}}$, we estimated that the axial frequency should be

$$f = \frac{c_0}{2\pi R\sqrt{\varepsilon_{\mathrm{effective}}}} \approx 530\ \mathrm{GHz}. \tag{6}$$

B. Computation Method

The EM simulation was conducted using the CST Microwave Studio software package, utilizing a 3-D finite-difference or finite-element analysis to solve Maxwell's equations over a mesh of cells covering the model. The simulation of the model followed a similar pattern to our previous work [13]. However, we used the T-solver instead of F-solver (i.e., time domain and not frequency domain). The source we used is a plane wave perpendicular to the skin surface, where the impinging electric field is a 1 V/m field, as shown in Fig. 9 below. Using such a source, eliminated possible parasitic effects due to the creation of a standing wave between the model surface and the port.

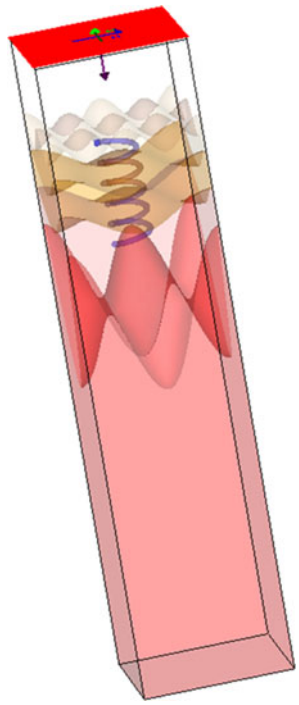

Fig. 9. Impinging plane wave. The electric field is 1 V/m.

TABLE II
DENSITIES OF THE SKIN LAYER MODEL

Layer	$\rho(\frac{kg}{m^3})$
Epidermis (SC,ME, and IE)	1200
Dermis	1200
Sweat duct wall	750

Densities of the skin layer model, for both, the thin and the thick models.

Another feature employed to increase the efficiency of the mesh, while maintaining an acceptable computational load, was the application of aperiodic boundary condition to the model. Effectively this allows the application of Floquet's theorem for periodic structures [13], [26], reducing computation time and removing boundary effects from the result. However, such a scheme necessitates a plane wave as the incident radiation.

The emphasis of this research was on SAR values. Although these values can depend on the orientation of the impinging E-field, it is enough to consider a perpendicular wave to observe gross tendencies in the frequency dependence of SAR.

Based on the electric field distributions, SARs simulation was performed. The SAR is defined as the time derivative of the incremental energy (dW) absorbed by (dissipated in) an incremental mass (dm) contained in a volume element (dV) of a given mass density (ρ)

$$\mathrm{SAR} = \frac{d}{dt}\left(\frac{dW}{dm}\right) = \frac{d}{dt}\left(\frac{dW}{\rho \cdot dV}\right). \tag{7}$$

In our simulations ,we used Point SAR, i.e., local SAR without mass or volume averaging.

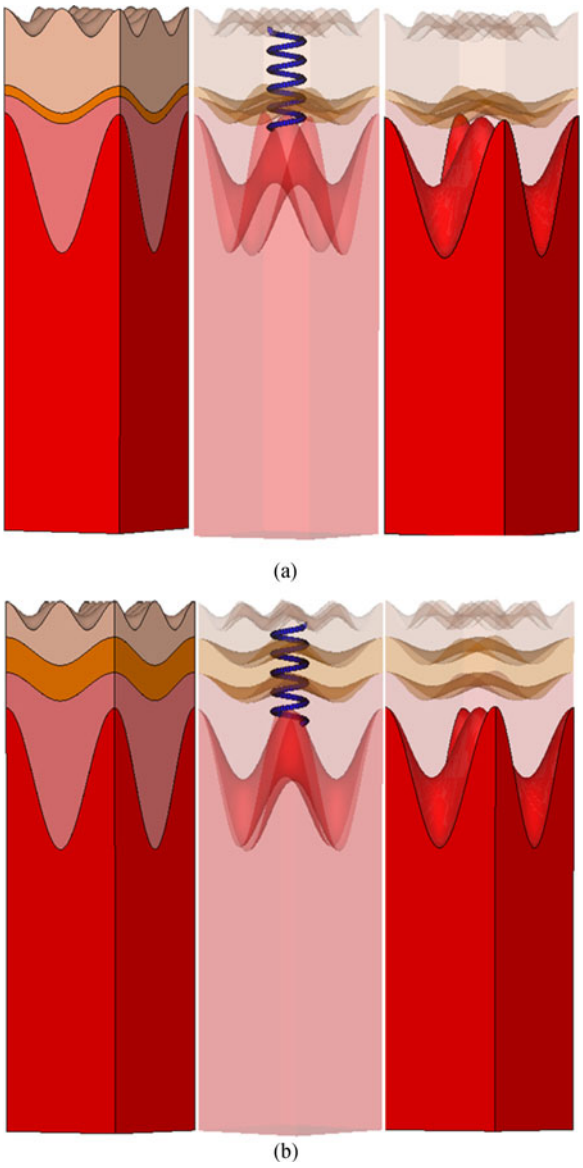

Fig. 10. (a) *Thick skin*. On the left is the model. In the middle is a transparent figure of the model. The helical sweat duct is embedded in the epidermis. On the right is the model with no sweat duct. (b) *Thin skin*. On the left is the model. In the middle is a transparent figure of the model. The helical sweat duct is embedded in the epidermis. On the right is the model with no sweat duct.

The densities, ρ, of the skin layers are described in Table II [27]. The value given for the sweat duct represents an averaged density between the duct wall and the aqueous content, considered as having the same density as sea water (995 Kg/m^3).

In order to check the dependence of the radiation absorption on skin type, we simulated SARs for thin skin and for thick skin. Fig. 10(a) and (b) shows the different skin-type models, where for each type we changed the ducts' conductivity: 2000, 5000, 10 000 S/m and no duct. These values of duct ac conductivity have been previously justified [13]. The different conductivities of the sweat duct correspond to different activity level of the sweat gland, i.e., high conductivity corresponds to high activity of the gland [13]. Fig. 10(b) shows the same methodology for the thin skin type.

TABLE III
PHYSICAL DIMENSIONS OF THE SKIN LAYER TYPES

Layer	Thin Skin	Thick Skin
SC Thickness μm	100	220
ME Thickness μm	100	30
IE Thickness μm	100	50
Dermis thickness μm	1000	1000
Effective dielectric permittivity	3.18	2.88
Axial frequency GHz	3.18	2.88

The physical dimensions of the thick and thin skin models, the effective permittivity and the axial frequency.

Table III below contains the physical dimensions on the thick and thin skin models, the effective dielectric permittivity and the axial frequency, where the last two flat was calculated for the thick skin model using the method we used and described previously for the thin skin model.

IV. RESULTS AND DISCUSSION

The SAR distributions for $f = 440$ GHz are described in Fig. 11, panels (a) and (b), for the thin skin model and in Fig. 12 for the thick skin model. In both cases the same model is presented without the presence of the sweat duct for comparison [see panels (c) and (d)]. The effect of the sweat duct is unmistakable in both cases, presenting as it does a conduit for the absorption of EM energy in the skin layer. The cut away [see panel (b)] clearly demonstrates the high level of SAR in the sweat duct, compared to the surrounding tissue. This energy is dissipated along the boundary of the epidermis with the dermis.

While the current model does not take into consideration heat perfusion in the epidermal layer, this is not expected to significantly affect the result, as heat transport in this layer is poor [27]. In Figs. 13 and 14, the maximum values of SAR are plotted as a function of frequency and of duct conductivity for the two models, respectively. As a comparison, the maximal SAR is also plotted for the same models lacking the sweat duct. As expected, these comparison curves are flat. Values as high as 1.8 W/kg were achieved for frequencies above 350 GHz. These can be compared to the FDA SAR limits for medical imaging limit head exposure to 3.2 W/kg averaged over 10 min [28], indicating a very real concern.

The two models exhibit strong peak at 410 and 500 GHz for the thick skin model and 440 and 580 GHz for the thin skinned model, respectively. These peaks represent the optimal frequencies for absorbance and their peak frequencies should coincide with the prediction of (6). However, there are significant differences. One possibility could be that the prediction should not be for circular polarization, but rather bound by the limits $3c/(4\pi d\sqrt{\varepsilon}) \leq f \leq 4c/(3\pi d\sqrt{\varepsilon})$ [18].

This yields 400 GHz $\leq$ f depending on the ellipticity of the polarization and using the diameter of the helix ($\sim$100 μm), this dovetails to the finding of circular dichroism in [14]. Interestingly, the lower frequency does coincide with the prediction of [18], based on an effective layer permittivity of $\varepsilon_{\text{effective}} = 5.1$ derived from skin reflections of a time domain THz pulse.

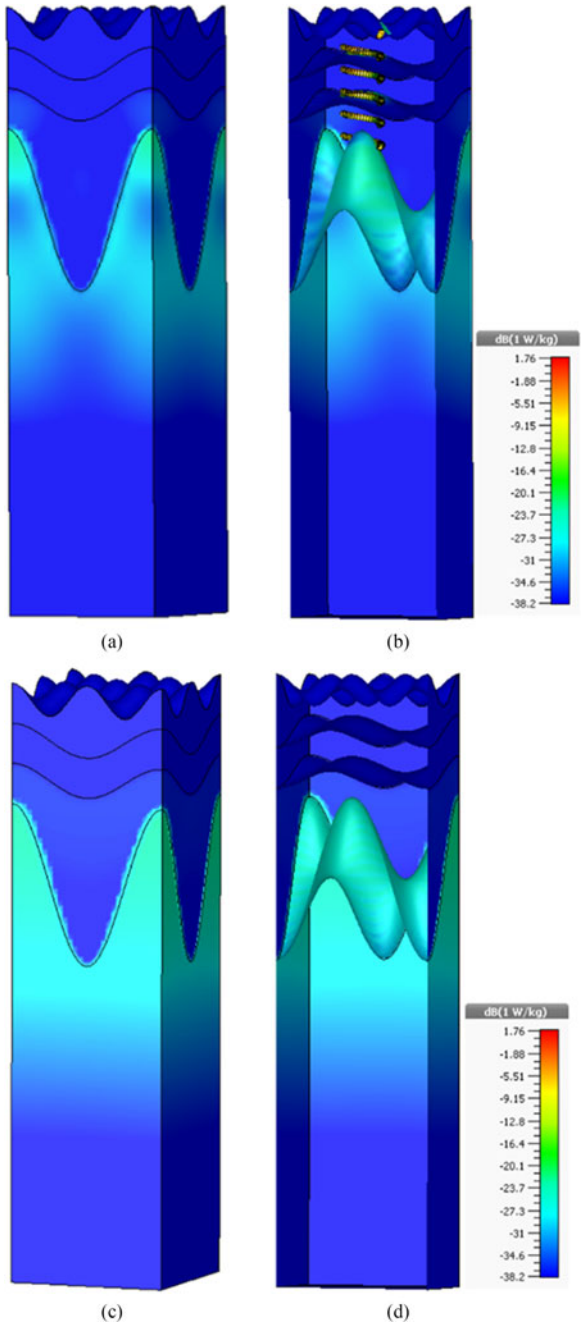

Fig. 11. SARs distribution patterns over the model calculated at a frequency of 440 GHz with a duct ac conductivity of 10 000 S/m, (a) for the thin skin model Fig. 10(b), (b) the same model showing a cross section exposing the sweat duct, (c) for the thin skin model without an embedded sweat duct, and (d) The cross section of the same ductless model. Red indicates a high SAR value of above 1.76 W/kg in dB, and blue a low SAR value. The simulation indicates that the main mechanism for sub-THz absorption in the skin layer is via absorption in the duct.

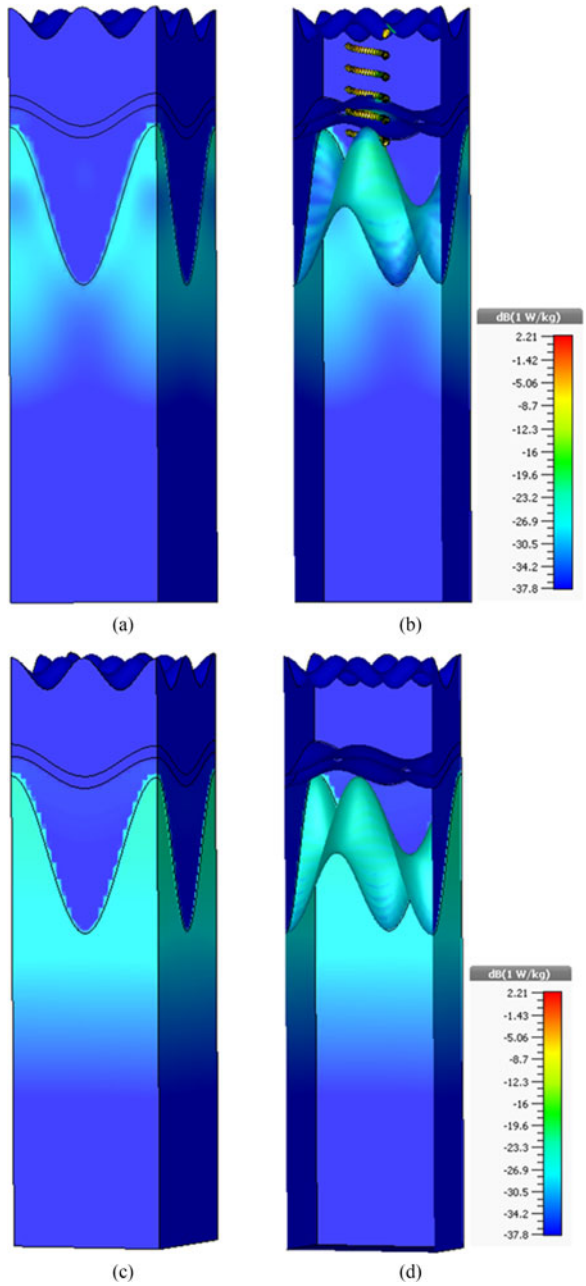

Fig. 12. SAR distribution patterns for the thick skin model calculated at a frequency of 450 GHz and a duct ac conductivity of 10 000 S/m, (a) for the model with an embedded sweat duct, (b) a cross section of the same model showing the position of the sweat duct, (c) the same model without the presence of a duct, and (d) a cross section of the same model. Red indicates a SAR value of above 2.2 W/kg in dB, and blue a low SAR value. The results tally with those of the thin skin model, showing the energy is preferentially absorbed in the duct.

However, this value of permittivity cannot be reconciled to the values of layer permittivity used for our model (see Table I). If, rather than (6) for the axial mode of a helical antenna, one considers the condition for a standing wave in the epidermis

$$f = \frac{c_0}{\pi d \sqrt{\varepsilon_{\text{effective}}}} \tag{8}$$

where c_0 is the speed of light and d is the layer dimension, then the two peak frequencies correspond to an effective maximum and minimum dimensions of the boundary between the dermis and the epidermis from the skin surface with $d_{\min} = 330\ \mu$m and $d_{\max} = 410\ \mu$m, based on the effective permittivity of the epidermis estimated from (4) ($\varepsilon_{\text{effective}} = 3.21$).

The influence of the ac conductivity of the duct is clearly evident in Fig. 13 (thin skin) and Fig. 14 (thick skin), it is clear

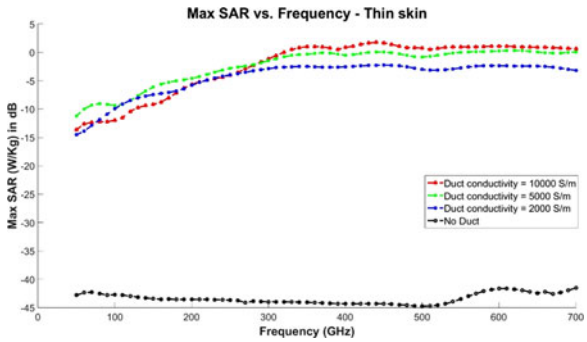
Max SAR vs. Frequency - Thin skin
Max SAR (W/Kg) in dB
Frequency (GHz)
Duct conductivity = 10000 S/m
Duct conductivity = 5000 S/m
Duct conductivity = 2000 S/m
No Duct

Fig. 13. Maximal SAR as a function of the frequency for thin skin.

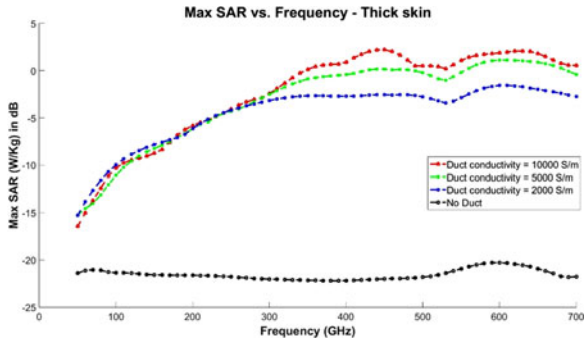
Max SAR vs. Frequency - Thick skin
Max SAR (W/Kg) in dB
Frequency (GHz)
Duct conductivity = 10000 S/m
Duct conductivity = 5000 S/m
Duct conductivity = 2000 S/m
No Duct

Fig. 14. Maximal SAR as a function of the frequency for thick skin.

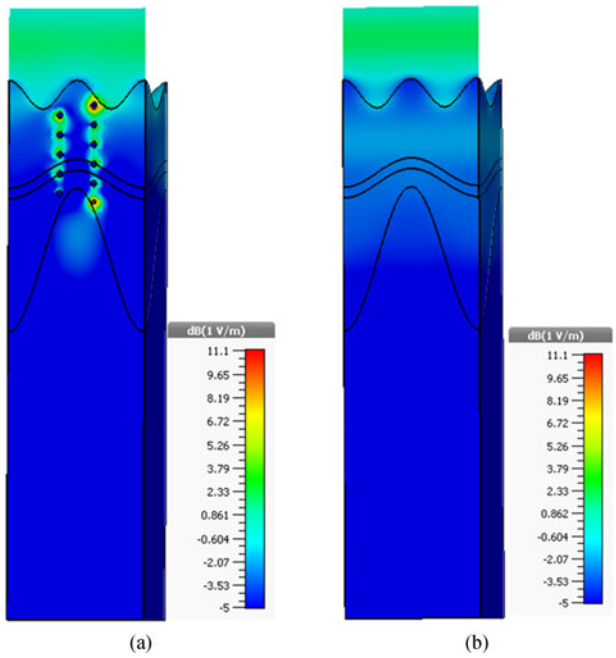

Fig. 15. Cross-section of the E-field of a thick skin in frequency of 450 GHz. (a) Model with duct. Red indicates an E-field of value 11.1 V/m in dB (b) Model without duct.

that at even low levels of 2000 S/m, the level of SARs is still high.

These conclusions are further accentuated when one visualizes the electric field distributions inside the model (see Figs. 15 and 16). The EM field concentrates in the duct where it is effectively absorbed.

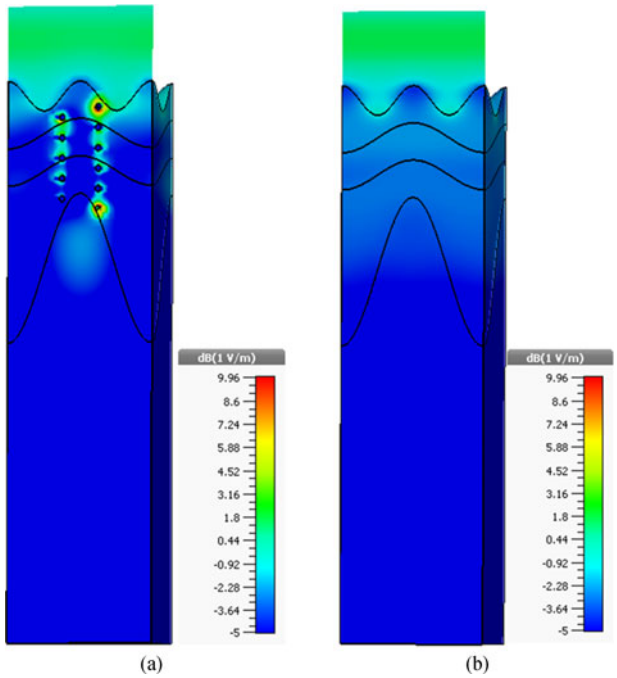

Fig. 16. Cross section of the E-field of a thin skin in frequency of 450 GHz. (a) Model with duct. Red indicates an E-field of value 9.96 V/m in dB. (b) Model without duct.

V. Conclusion

The need for high data transmission rates, coupled with advances in semiconductor technology, is pushing the communications industry toward the sub-THz frequency spectrum. While this is a relatively underutilized area of the EM spectrum, it does come with a price. The affinity of atmospheric absorption in this band means that many small short range and relatively powerful transmitters will be required for decent coverage. The results of our study emphasize that rather than gallop toward these solutions with abandon, the human health implications must be considered first, as wavelengths approach the dimensions of skin-based features. The results point to the dominant role of the sweat duct in EM skin absorbance. We can conclude and say that if the new regime of WLAN communication, the 5G standard, will happen in the next years, the concern regarding biological influence on the human body should be considered.

References

[1] T. Kürner and S. Priebe, "Towards THz communications - status in research, standardization and regulation," *J. Infrared Millim. THz Waves*, vol. 35, no. 1, pp. 53–62, Jan. 2014.

[2] G. C. Walker, E. Berry, S. W. Smye, and D. S. Brettle, "Materials for phantoms for terahertz pulsed imaging," *Phys. Med. Biol.*, vol. 49, no. 21, pp. N363–N369, Nov. 2004.

[3] C. Reid, A. P. Gibson, J. C. Hebden, and V. P. Wallace, "The use of tissue mimicking phantoms in analysing contrast in THz pulsed imaging of biological tissue," in *Proc. 2007 Joint 32nd Int. Conf. Infrared Millim. Waves 15th Int. Conf. THz Electron.*, 2007, pp. 567–568.

[4] N. Pałka, R. Ryniec, M. Piszczek, M. Kowalski, E. Rurka, and M. Szustakowski, "Construction and evaluation of the terahertz human phantom," *Przegląd Elektrotechniczny*, vol. 6, pp. 248–251, 2013.

[5] Y. Feldman, A. Puzenko, P. Ben Ishai, A. Caduff, and A. J. Agranat, "Human skin as arrays of helical antennas in the millimeter and submillimeter wave range," *Phys. Rev. Lett.*, vol. 100, no. 12, Mar. 2008, Art. no. 128102.

[6] Y. Feldman *et al.*, "The electromagnetic response of human skin in the millimetre and submillimetre wave range," *Phys. Med. Biol.*, vol. 54, no. 11, pp. 3341–3363, Jun. 2009.
[7] T. Nagaoka and S. Watanabe, "Voxel-based variable posture models of human anatomy," *Proc. IEEE*, vol. 97, no. 12, pp. 2015–2025, Dec. 2009.
[8] T. Nagaoka *et al.*, "Development of realistic high-resolution whole-body voxel models of Japanese adult males and females of average height and weight, and application of models to radio-frequency electromagnetic-field dosimetry," *Phys. Med. Biol.*, vol. 49, no. 1, pp. 1–15, Jan. 2004.
[9] P. J. Dimbylow, "FDTD calculations of the whole-body averaged SAR in an anatomically realistic voxel model of the human body from 1 MHz to 1 GHz," *Phys. Med. Biol.*, vol. 42, no. 3, pp. 479–490, 1997.
[10] "AustinMan Electromagnetic Voxels v2.2." [Online]. Available: http://web2.corral.tacc.utexas.edu/AustinManEMVoxels/AustinMan/download/AustinMan_v2-2.html. Accessed on: Jan 11, 2017.
[11] J. W. Massey, V. Subramanian, C. Liu, and A. E. Yılmaz, "Analyzing UHF-band antennas near anatomical human models with a fast integral-equation method," in *Proc. 2016 10th Eur. Conf. Antennas Propag.*, 2016, pp. 1–5.
[12] B. Querleux, *Computational Biophysics of the Skin*. Boca Raton, FL, USA: CRC Press, 2016.
[13] I. Hayut, A. Puzenko, P. Ben Ishai, A. Polsman, A. J. Agranat, and Y. Feldman, "The helical structure of sweat ducts: their influence on the electromagnetic reflection spectrum of the skin," *IEEE Trans. THz Sci. Technol.*, vol. 3, no. 2, pp. 207–215, Mar. 2013.
[14] I. Hayut, P. Ben Ishai, A. J. Agranat, and Y. Feldman, "Circular polarization induced by the three-dimensional chiral structure of human sweat ducts," *Phys. Rev. E*, vol. 89, no. 4, Apr. 2014, Art. no. 042715.
[15] "The remote sensing of mental stress from the electromagnetic reflection coefficient of human skin in the sub-THz range. - PubMed - NCBI." [Online]. Available: https://www.ncbi.nlm.nih.gov/pubmed/22170380, Accessed on: Aug. 21, 2017.
[16] G. Shafirstein and E. G. Moros, "Modelling millimetre wave propagation and absorption in a high resolution skin model: the effect of sweat glands," *Phys. Med. Biol.*, vol. 56, no. 5, pp. 1329–1339, Mar. 2011.
[17] B. Yang, R. S. Donnan, M. Zhou, and A. A. Kingravi, "Reassessment of the electromagnetic reflection response of human skin at W-band," *Opt. Lett.*, vol. 36, no. 21, pp. 4203–4205, Nov. 2011.
[18] S. R. Tripathi, E. Miyata, P. Ben Ishai, and K. Kawase, "Morphology of human sweat ducts observed by optical coherence tomography and their frequency of resonance in the terahertz frequency region," *Sci. Rep.*, vol. 5, 2015, Art. no. 9071.
[19] P. F. Millington and R. Wilkinson, *Skin*, 1 Reissue ed. Cambridge, U.K.: Cambridge Univ. Press, 2009.
[20] F. M. Watt, "Terminal differentiation of epidermal keratinocytes," *Current Opinion Cell Biol.*, vol. 1, no. 6, pp. 1107–1115, Dec. 1989.
[21] M. Egawa, T. Hirao, and M. Takahashi, "In vivo estimation of stratum corneum thickness from water concentration profiles obtained with raman spectroscopy," *Acta Dermato Venereologica*, vol. 87, no. 1, pp. 4–8, Jan. 2007.
[22] R. Gulich, M. Köhler, P. Lunkenheimer, and A. Loidl, "Dielectric spectroscopy on aqueous electrolytic solutions," *Radiat. Environ. Biophys.*, vol. 48, no. 1, pp. 107–114, Feb. 2009.
[23] J. Kim, W. Lu, W. Qiu, L. Wang, M. Caffrey, and D. Zhong, "Ultrafast hydration dynamics in the lipidic cubic phase: Discrete water structures in nanochannels," *J. Phys. Chem. B*, vol. 110, no. 43, pp. 21994–22000, Nov. 2006.
[24] A. F. Abdelaziz, Q. H. Abbasi, K. Yang, K. Qaraqe, Y. Hao, and A. Alomainy, "Terahertz signal propagation analysis inside the human skin," in *2015 IEEE 11th Int. Conf. Wireless Mobile Comput., Netw. Commun.*, 2015, pp. 15–19.
[25] R. Pethig, "Dielectric properties of body tissues," *Clin. Phys. Physiol. Meas.*, vol. 8, Suppl. A, pp. 5–12, 1987.
[26] W. Magnus and S. Winkler, *Hill's Equation*. Mineola, NY, USA: Dover, 2004.
[27] T. Gowrishankar, D. A. Stewart, G. T. Martin, and J. C. Weaver, "Transport lattice models of heat transport in skin with spatially heterogeneous, temperature-dependent perfusion," *Biomed. Eng. OnLine*, vol. 3, p. 42, 2004.
[28] C. for D. and R. Health, "Search for FDA guidance documents—Criteria for significant risk investigations of magnetic resonance diagnostic devices—Guidance for Industry and Food and Drug Administration Staff." [Online]. Available: https://www.fda.gov/RegulatoryInformation/Guidances/ucm072686.htm. Accessed on: May 24, 2017.

Noa Betzalel received the B.Sc. degree in electrical and computer engineering specialized in microelectronics and optoelectronics, and M.Sc. degree in applied physics from the School of Computer Science and Engineering, The Hebrew University of Jerusalem, Jerusalem, Israel. She is currently working toward the Ph.D. degree at the Department of Applied Physics, School of Computer Science and Engineering, The Hebrew University of Jerusalem.

Her current work is focused on sub-THz and THz frequencies technologies and remote biosensing from human skin at these frequency bands.

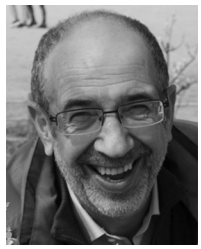

Yuri Feldman received the M.S. degree in radio physics and Ph.D. degree in molecular physics from the Kazan State University, Kazan, Russia, in 1973 and 1981, respectively.

From 1973 to 1991, he was with the Laboratory of Molecular Biophysics, Kazan Institute of Biology, Academy of Science of the USSR. In 1991, he joined The Hebrew University of Jerusalem, Jerusalem, Israel, where he is currently a Full Professor and the Head of the Soft Condensed Matter Physics Laboratory. He is the Director of the Centre for Electromagnetic Research and Characterization. He has spent over 40 years in the field and has authored or co-authored more than 400 scientific publications related to dielectric spectroscopy and its applications. He holds 15 patents in the areas of electromagnetic properties of the matter. His current research interests include broadband dielectric spectroscopy in frequency and time domains, theory of dielectric polarization and relaxation, relaxation phenomena and strange kinetics in disordered materials, and electromagnetic properties of biological systems *in vitro* and *in vivo*.

Prof. Feldman is a member of the Boards of International Dielectric Society and the International Society for Electromagnetic Aquametry. In 1992 and 2010, he was the recipient of an award for the outstanding contribution to the development of Israel Science by the Israel Government, and in 1998, he was the recipient of the Kaye Award for the best innovation and invention.

Paul Ben Ishai joined the Physics Department, Ariel University, Ariel, Israel, in 2016 after heading the Center of Electromagnetic Research and Characterization, Hebrew University, for the last 12 years. During this time, he concurrently worked with the laboratory of Prof. Feldman, where he concentrated on dielectric research. His research interests include soft condensed matter physics, glassy dynamics, biophysics, sub terahertz spectroscopy, and dielectric spectroscopy. In 2004, he was part of the founding team investigating the interaction of the human sweat duct with sub terahertz electromagnetic radiation, research that he is still involved with today.